Postmidnight equatorial plasma irregularities on June solstice during low solar activity – a case study

Claudia M N Candido[1,2], Jiankui Shi[1], Inez S. Batista[2], Fabio Becker-Guedes[2], Emília Correia[2,6], Mangalathayil A. Abdu[2,4], Jonathan Makela[3], Nanan Balan[7], Narayan Chapagain[5], Chi Wang[1], Zhengkuan Liu[1]

[1]National Space Science Center, NSSC, Chinese Academy of Sciences, State Key Laboratory, China-Brazil Joint Laboratory for Space Weather, China

[2]National Institute for Space Research – INPE, - São José dos Campos, SP, Brazil

[3]Department of Electrical and Computer Engineering, University of Illinois at Urbana-Champaign, Urbana, Illinois 61801, U.S.A

[4]Instituto Tecnológico de Aeronáutica – ITA – São Jose dos Campos, Brazil

[5]Departament of Physics, Patan Multiple Campus, Tribhuvan University, Latitpur, Nepal.

[6]Centro de Radio Astronomia e Astrofísica Mackenzie, CRAAM, University Presbiteriana Mackenzie – São Paulo – Brazil

[7]Institute of Geology and Geophysics, Chinese Academy of Sciences, Beijing, China

Corresponding author: claudia.candido@inpe.br

Keywords: Solar minimum, Spread-F, Postmidnight plasma irregularities, equatorial ionosphere, ionosonde, ionospheric forecast

Abstract

We present a case study of unusual spread-F structures observed by ionosondes at two equatorial and low latitude Brazilian stations - Sao Luis (SL: 44.2° W, 2.33° S, dip angle: −6.9°) and Fortaleza (FZ: 38.45°W, 3.9° S, dip angle: −16°). The irregularity structures observed from midnight to post-midnight hours of moderate solar activity (F10.7 < 97 sfu, where 1sfu = 10^{-22}W.m^{-2}.s^{-1}) have characteristics different from typical post-sunset equatorial spread-F. The spread-F traces first appeared at or above the F-layer peak and gradually became well-formed mixed spread-F. They also appeared as plasma depletions in the 630.0 nm airglow emissions made by a wide-angle imager located at nearby low latitude station Cajazeiras (CZ: 38.56° W, 6.87° S, dip angle: -21.4°). The irregularities appeared first over FZ and later over SL, giving evidence of an unusual westward propagation or a horizontal plasma advection. The drift mode operation available in one of the ionosondes (a Digital Portable Sounder, DPS-4) has enabled us to analyze the horizontal drift velocities and directions of the irregularity movement. We also analyzed the neutral wind velocity measured by a Fabry-Perot interferometer (FPI) installed at CZ and discussed its possible role in the development of the irregularities.

1 Introduction

Equatorial spread-F representing small-scale to large-scale plasma irregularities, has been extensively studied for several decades. The large-scale plasma irregularities, specifically known as equatorial plasma bubbles (EPBs), are known to be associated with equatorial spread-F. In the Brazilian equatorial sector, characterized by large negative magnetic declination, spread-F and EPBs have high occurrence rates during local summer and equinoctial months (Abdu et al., 1981a; Sahai et al., 2000; Sobral et al., 2002). However,

during low solar activity conditions, there is a class of spread-F/plasma irregularities regularly observed in distinct longitudinal sectors, such as Brazil (Candido et al., 2011), Africa (Yizengaw et al., 2013), and Asia (Nishioka et al., 2012). They are known as post-midnight plasma irregularities (PMIs), which occur mostly in June solstice. Comprehensive reviews on post-midnight plasma irregularities and plasma irregularities have been recently published by Otsuka (2017) and Balan et al. (2018).

PMIs occur under conditions considered not favorable for the development of the Rayleigh-Taylor (RT) instability, since that at night the vertical plasma drifts are downward, owing to the westward electric fields. In recent years, a variety of works have reported their occurrence both at low latitudes and the equatorial region. Otsuka et al. (2009) and Nishioka et al. (2012) investigated PMIs over Indonesia and discussed their possible sources. Li et al. (2011) reported these irregularities observed over Hainan, China, during low solar activity. Candido et al. (2011) presented a study of PMIs observed over the south crest of the equatorial ionization anomaly (EIA) during low solar activity, in CP, Brazil. Yokoyama et al. (2011) studied unusual patterns of echoes from coherent scatter radar data occurring around midnight during the solar minimum period. They observed two principal types of irregularities: the upwelling plumes and MSTID-like striations. They have argued that the former can be generated by both the RT instability (at equatorial region) or the Perkins instability (at mid-latitude region) and the later only by the Perkins instability. Yizengaw et al. (2013) presented the study of the PMIs over equatorial Africa and also investigated their most probable causes. Dao et al. (2016) reported the occurrence of postmidnight field-aligned irregularities (FAIs) in Indonesia during low solar activity in 2010.

Many instrumental techniques are currently providing high-quality measurements and results for ionospheric studies. Early investigations of the ionosphere referred to the diffuse echoes seen in data from measurements using ionosondes, which are high-frequency radars

used for ionospheric sounding (Breit and Tuve, 1926; Booker and Wells, 1938). The "spread-F" is widely used to generically refer to the irregularities observed in the equatorial and low-latitude regions. Nowadays, digital ionosondes are extensively used for ground-based sounding of the ionosphere, providing information from the E-region to the peak of the F-layer, over a variable range of frequencies as well as features related to the propagation of the irregularities (Reinisch et al., 2004; Batista et al., 2008, Abdu et al., 2009). Equatorial spread-F has been extensively studied for several decades, and it is known to be associated with the occurrence of large-scale plasma irregularities or equatorial plasma bubbles (EPBs).

Optical imaging of thermospheric emissions, like that used in this work, is also a useful ground-based technique for studying thermosphere/ionosphere processes. All-sky imaging systems provide images of thermospheric emissions (e.g., OI 630-nm, OI 777.4-nm emissions) at ionospheric heights over a large horizontal extent. The OI 630-nm emission comes from recombination processes between molecular oxygen and electrons and presents a volumetric emission rate which peaks at an altitude of ~250 km, around the F-layer the bottom side height. In this way, variations in the intensity of the emission (dark and bright regions) are used as tracers of ionospheric irregularities, such as EPBs, or other disturbances, such as travelling ionospheric disturbances - TIDs (Pimenta et al., 2008; Abalde et al., 2009; Makela et al., 2010; Candido et al., 2011; Chapagain et al., 2012).

For clarity for the present study, which presents a distinct pattern of spread-F from those usually observed in equatorial ionograms, we first address the current state of understanding regarding spread-F signatures in ionosonde data.

It is currently accepted that there are two main spread-F types: range and frequency type spread-F traces (Abdu et al., 1998). The range type spread-F, often associated with the occurrence of medium and large-scale irregularities, including EPBs, is comprised of trace

patterns with the echoes spread in range and with the onset beginning at the lower frequency end of the F-layer trace in ionograms. During the spread-F season in Brazil, between October and March, the evening pre-reversal enhancement in the zonal electric field, and therefore the F-layer vertical drift, attains large values and range type spread-F is observed in equatorial ionograms, followed by their appearance at crest region of the EIA, which is located around Cachoeira Paulista (CP: 22.4° S, 45° W, dip angle: -37°). During the remaining part of the year, when the vertical drifts are minimal (Batista et al., 1996), spread-F is restricted to the height region below the F-layer peak, rarely reaching the topside ionosphere, and therefore observed only close to the dip equator. This type of spread-F is usually classified as bottom side spread-F (Valadares et al., 1983). The other typical spread-F pattern observed in equatorial ionograms is the frequency type spread-F. In this case, the spread-F echoes are seen at frequencies around the F-layer critical frequency (foF2). It is believed to be associated with smaller scale/decaying irregularities following spread-F/EPBs (Abdu et al., 1981b).

Some studies have pointed out that frequency type spread-F can sometimes be associated with patches of ionization propagating eastward (MacDougall et al., 1998). However other spread-F patterns are frequently observed in solstices in distinct longitudinal sectors as reported in Brazilian (Candido et al., 2011, MacDougal et al., 2011), Asian (Yokohama et al., 2011), African (Yinzengaw et al., 2013), and Peruvian (Zhan et al., 2018) sectors. Also, it is known that both frequency and range spread-F types can appear simultaneously, as a mixed spread-F pattern. In this work, we present a case study on an unusual/anomalous spread-F/plasma irregularities/depletions pattern observed over the equatorial region. We use the term “unusual” in the sense that the observed features are distinct from those typically observed for spread-F associated with post-sunset spread-F, as described above. Although the unusual type of spread-F has been recognized since the early studies of the

equatorial ionosphere (Munro and Heisler, 1956; Heisler, 1958; Calvert and Cohen, 1961; Bowman, 2001), this is the first time that it is reported for the Brazilian equatorial region with simultaneous airglow observations, which reveal important ionospheric characteristics not available when using only ionosonde data. The earlier studies extensively reported the occurrence of anomalies in F-layer traces, such as cusps, F2 forking, and their possible association with TIDs. Calvert and Cohen (1961) presented a comprehensive study of the distinct spread-F patterns. They concluded that the distinct configurations or shapes of spread-F were associated with the scattering in the vertical east-west plane from field-aligned irregularities and that the spread-F pattern depends on the position relative to the ionosonde and the scale sizes of the irregularities.

2. Data and Method

2.1 Digisondes

We analyzed ionograms from two Digisondes DPS-4 operated at two Brazilian equatorial sites: SL (44.2° W, 2.33° S, dip angle: −6.9°) and FZ (38.45° W, 3.9° S, dip angle: −16°), which are separated in the east-west direction by ~600 km. Both instruments provided ionograms at a 10-minute cadence. The DPS-4 also performs echo directional studies based on Doppler interferometry, which provides information about the drift velocities associated with irregularities. The operation of each Digisonde is based on the transmission of pulses at digital frequencies from 1 to 20 MHz that are reflected from the ionosphere at plasma frequencies lower than foF2. The maximum height range of the ionograms can be set at ~700 or ~1400 km, for which the resolution is ~5 km and ~10 km, respectively. The ionospheric true heights are calculated by an inversion method implemented by the ARTIST

155 software (Reinisch et al., 2005). Manual scaling of the data can be performed by editing the
156 ionograms using the SAO Explorer software (Galkin et al., 2008). The interferometry
157 system used by the Digisondes receiver is comprised of four small-spaced antennas for
158 signal reception arranged in a triangle with one antenna at the center. The signals from each
159 antenna are Fourier analyzed to identify echoes with different Doppler frequencies (for more
160 details, see Reinisch et al., 2004). The Drift Explorer software determines the location of the
161 source regions of the spread-F echoes for each Doppler component. The ionograms present a
162 color code showing the direction of echoes that form the spread-F. The sky map and drift
163 data collected after the ionogram are derived from the measured Doppler frequency and
164 angle of arrival of reflected echoes. Special processing software enables us to plot skymaps
165 showing the location of all reflection sources. The Drift Explorer also provides plots of the
166 drift velocities (zonal, vertical, and meridional components). For more details about
167 Digisondes sounding modes and drift measurements see Reinisch et al. (2005) and
168 references therein.
169
170 **2.2 Wide-Angle Imaging System**
171 The airglow images of the OI 630-nm emission used in this study were measured by a
172 Portable Ionospheric Camera and Small-Scale Observatory (PICASSO) wide-angle imaging
173 system deployed at Cajazeiras (CZ: 6.87° S, 38.56° W, dip angle: -21.4°), located about
174 ~352 km to the south of FZ. It is a miniaturized imaging system that measures the 630.0-nm
175 and 777.4-nm nightglow emissions. Since the 777.4-nm emission is generally very weak
176 during solar minimum conditions, we use only the 630.0-nm emission image data for this
177 study. The PICASSO images are captured on a 1024 × 1024 Andor DU434 CCD with a
178 spatial resolution of approximately 1 km (azimuthal) over the entire field of view. The
179 spatial resolution in the radial direction varies from ~1 km to ~5 km from zenith to the edge

of the field of view. The noise contributions from dark current are reduced by cooling the CCD to at least -60°C. The exposure time for each image is 90 s, and dark images are taken frequently to remove noise and read-out biases. For details about the data processing from a similar PICASSO installation, see Makela and Miller (2008).

2.3 Fabry-Perot Interferometer (FPI)

FPIs are optical instruments that measure the spectral line shape of the 630.0 nm emission at around 250 km of altitude and are very useful to study thermospheric winds from Doppler shifts in the emission's frequency. For more details of the FPI technique, see Fisher et al. (2015) and references therein. The investigation of the departures of the background wind system can be useful to explain possible sources of the F-uplifts associated with late-time RT instability. For this purpose, we analyzed the behavior of the neutral winds over the equatorial region taken from a ground-based FPI installed in CZ.

3. Observations

3.1 Spread-F, F-layer height and plasma densities

We present a case study of a spread-F event which occurred in the June solstice of 2011 during a geomagnetically quiet (ΣKp = 11) night and low solar activity with mean F10.7 = 97 SFU (SFU is Solar Flux Unit = 10^{-22} W.m^{-2}.Hz^{-1}). Fig. 1 shows a sequence of ionograms on 25-26 July 2011 from 00:40 LT to 03:10 LT over SL (top panel) and over FZ low-latitude site (bottom panel) from 25 July 2011 at 22:00 LT to 26 July 2011 01:30 LT in which the presence of unusual spread-F patterns is observed. Over SL, the first spread-F

trace appears at 01:00 LT at an oblique angle close to or above the F-layer peak at a virtual range of 600 km. Over the next hour, this structure gradually moves closer to the station SL, finally merging with F-layer bottom side echoes and becoming a well-formed spread-F trace. During the spread-F development, it is possible to observe an apparent small increase in the F-layer heights. Finally, at the end of the spread-F event, around 02:50 LT, we observe a decreased foF2 and the appearance of an Es layer. We notice a very similar evolutionary pattern of the structures in the FZ ionograms as in those obtained from SL. However, the first spread-F traces appeared over FZ around 22:20 LT, much earlier than over the equatorial site, SL. These echoes from FZ lasted for about 3 hours. The spread-F echoes gradually move closer to the station or downward to form a well-structured spread-F pattern.

An important point to be considered is the local ionospheric background in which the spread-F occurred. The F-layer parameters, h'F (virtual height of the F-layer bottom side, in km), the hmF2 (the real height of the F-layer peak, in km) and foF2 (the F-layer critical frequency, in MHz) for both stations are shown in Fig. 2 from 18:00 LT to 06:00 LT. Over SL an uplift of the F-layer was observed between 21:00 LT and 23:00 LT, not associated with any spread-F echoes. Around 21:00 LT, at FZ, we may note some wave-like oscillations in the F-layer height (notable in hmF2) with a period on the order of one hour. The first spread-F trace at oblique angles (and perhaps above the F2 peak) appeared just after these oscillations, as shown by the blue lines connecting the h'F and hmF2 curves.

On the other hand, over FZ, where heights are lower than at SL, we observe stronger wave-like oscillations in both h'F and hmF2 three hours earlier than observed at SL. The F-layer critical frequency decreased for both stations, as it is expected for this period. At the beginning of the spread-F occurrence, the foF2 was as low as 4 MHz, corresponding to an electron density of 1.98×10^{5} el.cm^{-3}. The parameter fxI (not shown), or top frequency of

spread-F, which is the highest frequency of spread-F echoes, reached values not higher than 4.5 MHz over SL but reached values around 6.0 MHz over FZ, which means higher plasma density at this region. Moreover, after the spread-F ceased, it was possible to observe the recovery of the plasma frequency/density over FZ sooner than over SL, as shown in both panels around 05:30 LT.

3.2 Depletions in the airglow OI 630.0-nm emission

Figure 3 shows a sequence of four images of the OI 630.0-nm emission collected on 25-26 July 2011 at Cajazeiras (CZ: center of the frame), Brazil. The images are projected over a geographic map of Brazil assuming an emission altitude of 250 km. The sites of FZ and SL are also indicated in the images for reference. Between 23:12 LT to 01:26 LT at least two depletions (dark regions passing over FZ and CZ) can be observed propagating westward. These depletions propagated over FZ and CZ at 23:12 LT, in agreement with the spread-F traces seen in the ionograms from FZ.

3.3 F-layer irregularity Drifts – Directions and Velocities

Automatic drift mode routines were used to obtain information about the location of echo sources in the F-layer associated with plasma irregularities. These routines provide information about the distance of the reflected echoes, using measurements of the radar ranges to the vertical and oblique echoes as well as their directions, as described by Reinisch et al. (2004). The distribution of the echoes can be displayed in skymaps, as shown in Fig. 4. Skymaps between 00:12 LT and 00:42 LT were constructed using data from FZ during the spread-F event studied where reflected echoes appear and are distributed in a west-east elongated pattern covering a total horizontal distance of 1200 km (from west to east). It may

be noted that, in general, negative Doppler velocity (yellow color) of the echoes dominates the western azimuth while the eastern azimuth is dominated by positive Doppler velocity (blue color), a characteristic that is indicative of an overall westward motion of the irregularity structures. Additional directional information is obtained from the temporal evolution of each spread-F echo in plots of the horizontal distance of the echoes (horizontal axis) as a function of time (vertical axis), presented as directograms. A directogram for the night of 25-26 July 2011 constructed using data from FZ is shown in Fig. 5. Each horizontal line of the directogram corresponds to a single ionogram. The spread echoes are distributed at east and at west of the station mainly from 23:00 LT to ~ 01:00 LT, although there is a sparse distribution between 21:00 and 23:00 LT. The color codes at both sides indicate the location (at east or west) and the incoming and outgoing direction (arrows) of the reflectors (irregularities), for example, the first echoes are seen at the zonal distance of ~320 km between 23:00 and 23:30 LT coming from East (red squares). The color code indicates they are at the east of the station coming from the east side. Also, there are echoes at the east of the station which come from northeast, NNE, direction. Among these echoes, there are only a few points that are going eastward (blue points). From 23:30 to 01:30 LT, there are echoes at west, which gradually disappear after 02:00 LT. The color code to the left shows that they are at west from the station and going westward. Thus, the echoes present a mean westward propagation. We point out that the horizontal distance range limit is around 600 km, which correspond to an antenna beam angle of approximately 45°, as it is seen in the directograms on Fig. 5, and hmin is the spread-F reflection height.

The unusual spread-F echoes were observed at both equatorial sites, SL and FZ, with a zonal separation of ~600 km. The first spread-F trace was observed at 22:20 LT over FZ and later at 01:00 LT over SL. This lag of ~ 02:40 hours suggests an average westward drift velocity component of ~ 63 ms^{-1}. The DPS-4 drift mode provides the full-vector Doppler velocity for

the observed echoes. Figure 6 shows the variation of the Vz (vertical component) and V_y (zonal component) velocities taken from measurements of the Digisonde DPS-4 (drift mode) from 22:00 LT on July 25, 2011, to 04:00 LT on July 26, 2011. Positive (negative) V_y velocities represent eastward (westward) propagation. |V| represents the total drift Doppler velocities (<60 ms^{-1}), while the maximum vertical upward component is ~30 ms^{-1}. The zonal velocities inferred from Drift Explorer agree well with the estimate obtained from the difference in onset times of spread-F echoes between SL and FZ, with a mean value of ~55 ms^{-1} during the event. The middle panel is the vector diagram with the variations of the mean total electrodynamical drift velocity (see Balan et al., 1992). For clarity, the vector length is fixed, and the information on |V| is represented by the concentric circles (arrow start point). As it is observed, the vector is found to rotate anticlockwise, starting in the east-up sector in the night and reaching west-up sector in post-midnight. Velocities extracted from the airglow images obtained from CZ are shown in the bottom panel of Fig. 6. In order to estimate the velocity of the depletion structure, the individual images were processed by first spatially registering the 630.0-nm images using the star field. After removing the stars from the images using a point suppression methodology, the images were projected onto geographic coordinates assuming an airglow emission altitude of 250 km (for details of analysis technique see Chapagain et al., 2012). The depletion structure was selected in consecutive images to find the zonal shift of the structures from which the velocity was estimated. The estimated zonal propagation velocity was ~60 ms^{-1}, which agrees well with the velocities determined by the Doppler technique of the Digisonde. We should keep in mind that the Digisonde Doppler technique determines the mean irregularity motion while the velocities from the airglow technique estimate the mean propagation of the plasma depletion.

Besides the capabilities of the Digisonde to sound and detect the occurrence of plasma irregularities seen in the ionograms as spread-F echoes, and the F-region heights variations, and their vertical drifts, there is a method which uses the true heights to obtain information about the gravity waves oscillations at specific plasma frequencies. The true heights are extracted from virtual heights by an inversion algorithm used in the SAO Explore software. This method was described in detail by Abdu et al., 2009, in a comprehensive study about the influence of gravity waves on the equatorial spread-F. In their work, the same both locations were analyzed: the off-equator station FZ and the equatorial station SL. Because of both stations are more separated in longitude than in latitude, it was assumed that GW oscillations observed in the bottomside F-layer in FZ could have the same features at SL, considering few differences attributed to the magnetic field inclination in each one. In this work, we also took advantage of the simultaneous Digisonde sounding at these stations in order to verify the possible influence of GW as a precursor of the instability growth which leads to late development of spread-F studied.

Figure 7 presents the oscillations in F-layer true height at fixed frequencies (1.5-5.0 MHz) in both stations, SL and FZ. It is possible to observe oscillations prior to the development of spread-F especially in FZ, with periods around 1 hour, which will be discussed later in session 4.3.4

3.4 Thermospheric Winds

Figure 8 shows the measured thermospheric zonal (top panel) and meridional (bottom panel) wind on July 25-26, taken from the FPI installed in CZ, the same location where the airglow images were obtained. The shaded region encloses the standard deviation of the monthly average, the green lines are the average winds on July 25-26 (±2days), and the red line is the measurement for July 25-26. It is observed that on July 25-26 between 22:00 LT and 01:00

LT the zonal wind is abnormally eastward (~100 m/s), while the meridional wind departs from the monthly and daily variation average. From this, we can consider that a possible balance between the zonal and meridional wind component may be responsible by plasma advection (plasma movement) from low-latitude to equatorial region, which might have maintained the F-layer at a higher altitude as discussed by Nicolls et al., 2006. This apparent uplifts observed in both stations around 00:00 LT might have caused the growth of the late RT-instability and the PMIs.

4 Discussion

We present an unusual event of PMIs/spread-F/depletions over the equatorial site in Brazil that exhibits singular features. This is the first report of such distinct pattern of spread-F for the Brazilian equatorial region, though it was observed earlier at the low-latitude station CP (Brazil) for the solar minimum 2008-2009 by Candido et al., 2011. By distinct we mean that they occur in postmidnight hours, propagating westward, which is not usually observed during solar minimum unless there is a previous eastward EPB structure propagation, as mentioned by Paulino et al., 2010. A careful analysis of equatorial ionograms and other plots from digisonde soundings suggest modifications in the ionospheric plasma density structuring, such as those associated with plasma density depletions, which are responsible for a variety of spread F-layer patterns.

4.1 Depletions in the airglow OI 630.0 nm images

Airglow images show an apparent southwestward propagation of depletions on this night, which differs from the typical propagation direction of post-sunset EPBs. However, this

atypical propagation can be a characteristic of post-midnight depletions and needs further investigation with a long-term airglow database. The depletions also propagated over CZ (350 km south of FZ) with mean westward velocities ~60 ms^{-1} which are similar to the velocities of propagation of the irregularities observed with the Digisonde at FZ. Some authors have demonstrated that EPBs can also present westward propagation after midnight during quiet times (Paulino et al., 2010; Sobral et al., 2011). However, they defined in those studies that the depletions associated with EPBs should first present movement to the east earlier in the evening and reversal to westward at later hours. This is not the case for the structures presented in this work since there are no depletions in the OI 630.0-nm images propagating eastward earlier in the evening.

Moreover, Sobral et al. (2011), interpreted that westward traveling plasma bubbles (WTPB) observed in the same region were associated with westward zonal thermospheric winds (simulated results). On the other hand, Fisher et al. (2015) presented a climatological study of the quiet time thermospheric winds and temperatures by measurements of the OI 630.0 nm airglow emission spectral line shape over the same region. They noticed that during low solar activity (F10.7 < 125 sfu), the zonal and meridional winds are, on average, negligible in postmidnight hours. It is possible that these differences can be attributed to departures from the wind system at which could be responsible by the F-layer uplifts and plasma instabilities/irregularities development.

4.2 Spread-F in ionograms

As mentioned before, spread-F echoes in ionograms generally appear first at the low-frequency end, as satellite traces, evolving into spread-F echoes extended in frequency and range. These characteristics were not seen in the present study. In this work, the reflected echoes observed in the ionograms first came from oblique directions and at heights which

379 could be considered possibly higher than those observed overhead. The spread echoes
380 appear at the higher frequency edge of the F-layer, with top-frequency higher than the layer
381 critical frequency. Subsequently, the low-frequency edge of the cusp merges with the main
382 trace, while the baseline of the spread-F traces gradually decreases in height. Anomalous
383 traces in F-layer ionograms, such as 'cusps' or 'spurs,' were described in earlier studies to
384 be associated with traveling disturbances in the ionosphere. Munro and Heisler (1956) and
385 Heisler (1958) have observed the occurrence of anomalous traces in ionograms and
386 attributed them to the manifestations of TIDs. As it is well known, TIDs can be described as
387 frontal gravity waves propagating horizontally in the ionosphere, causing increases and
388 decreases in the ionization, i.e., horizontal gradients in the ionization. According to Munro
389 and Heisler (1956), changes in the ionization would be responsible for the anomalous traces
390 in the F-layer ionogram. Similar occurrences were reported by Ratcliffe (1956) for
391 ionograms from Huancayo, Peru. Calvert and Cohen (1961) have pointed out that some
392 spread-F traces observed over Huancayo presented characteristics similar to frequency
393 spread-F from "temperate" latitudes, which are mainly associated with TIDs. Also, they
394 studied distinct configurations of spread-F with echoes coming from oblique directions,
395 similar to what is presented in this work. The oblique echoes observed in ionograms alone
396 could not provide their zonal direction (from east or west). However, additional directional
397 information provided from the drift mode sounding of the Digisonde DPS-4 and their
398 appearance first in the ionograms over FZ followed by their occurrence over SL (a western
399 site in relation to FZ), suggested that they propagated westward. Late/pre-dawn spread-F
400 was also reported by McDougall et al. (1998) for solstices in the Brazilian sector. However,
401 they considered the occurrence of late time spread-F during December solstice at Fortaleza
402 as patches of ionization, which cause spread echoes at the high-frequency end or the

frequency spread-F. They also concluded that the echoes did not come from overhead structures but the east or west directions.

4.3 Post-midnight irregularities/F-region background conditions

As it is well-known, the poor alignment between the sunset terminator and the magnetic field lines during June solstice in Brazil is responsible by the low occurrence rate of post-sunset spread-F/EPBs, since the vertical plasma drifts are very weak. However, it is observed an occurrence peak of late night spread-F/plasma irregularities in June solstice, especially around midnight and post-midnight. For this, it is necessary to have an F-layer uplift, which creates favorable conditions for the development of the RT instability. These conditions are not entirely understood, and they have been discussed by several authors (McDougall et al., 1998; Nicolls et al., 2006; Abdu et al., 2009; Nishioka et al., 2012, Yokohama et al., 2011, Ajith et al., 2016).

During the high solar activity, the longitudinal variation of the declination angle is predominant on the F-layer vertical drift and the occurrence of the plasma irregularities, while it is not essential during solar minimum. During low solar activity/solar minimum, in the absence of geomagnetic disturbances, the seeding processes related to gravity waves seem to be more critical, especially when the PRE-amplitude is small or absent (Balachandran et al., 1992; Abdu et al., 2009). In this way, we should address the conditions which precede the occurrence of the post-midnight irregularities observed in this work. It is noticed that spread-F traces associated with plasma irregularities were detected firstly at oblique directions at least 500 km at east or west from the station, as seen in the directograms in Figure 5, which we can consider as ionospheric conditions favorable in a wide longitudinal range.

4.3.1 Thermospheric winds

Nicolls et al. (2006) discussed the nocturnal F-layer uplifts associated with the secondary maximum of spread-F occurrence rate in low solar activity. As it is well understood, the nocturnal westward electric field is responsible for the downward movement of the F-layer. During solar minimum, these electric fields can be easily reversed by a weak geomagnetic disturbance. However, in the absence of the geomagnetic disturbance, which is the case studied in this work, other sources should be considered. Analyzing F-layer uplifts for different conditions of solar activity, Nicolls et al. (2006) verified that during downward F-layer movement (decreasing westward electric field), even a small contribution of a meridional equatorward wind (~30m/s), could lead the F-layer to higher heights triggering the RT instability.

Moreover, it was discussed that neutral winds could not uplift the equatorial plasma directly, but they are sources of meridional advection (movement) of plasma, driven by a latitudinal gradient in electron density, responsible by F-layer uplifts. They concluded that the uplifts could be due to the decreasing, not to the reversal, of the westward zonal electric field associated with departures in the wind system related to the midnight temperature maximum (MTM), recombination processes, and the plasma flux. In this way, we analyze the zonal and the meridional neutral wind variation in Figure 8, in order to verify that there are suitable conditions for F-layer uplift. As it is observed in Figure 8 (top panel), the zonal wind is ~100 m/s just before midnight while meridional wind (equatorward) is ~30 m/s just after midnight (bottom panel). There is evidence that the mean equatorward meridional winds have kept the F-layer at higher altitudes enough to the trigger the RT instability development.

4.3.2 Recombination processes - Rayleigh Taylor instability growth rate

Nishioka et al. (2012) discussed the causes of the postmidnight uplifts that occurred during winter in Chumphon, Thailand (low latitude) and the post-midnight Field-Aligned Irregularities, FAIs, in Kototaband, Indonesia (equatorial region). As it is well known, the zonal electric field is westward during the night, as the vertical drift **ExB** is downward. This condition leads to a negative RT-instability growth rate. In this way, it is crucial to address, the importance of the term g/ν_{in} in the linear growth rate of RT-instability, and the recombination processes, as shown in Equation (1):

$$\gamma = \left(\frac{E}{B} + \frac{g}{\nu_{in}}\right)\frac{1}{L} \quad (1)$$

Where: E is the electric field; B is the magnetic field; g is the acceleration of gravity, ν_{in} is ion-neutral collision frequency; L is the scale length of the vertical gradient of the F-region plasma density. At night, the zonal electric field is westward, as the growth rate can be negative, i.e., the F-layer bottom side is stable. On the other hand, the term g/ν_{in} may increase in the following conditions: 1) ν_{in} is proportional to the neutral density, *n*, where *n* is smaller during the night than the day; 2) ν_{in} is smaller at higher altitudes owing to the decrease of *n* with the height; 3) ν_{in} is smaller during low solar activities. Therefore, under the appropriate conditions, the RT growth rate can be positive, although small, as it is observed in this work. To understand the recombination processes as a source of the F-layer uplift it should be considered that the F-layer bottom side is eroded if it is at lower altitudes (at ~300 km), such as there is a decreasing of peak density and the increasing of F-layer peak height. For clarity, we present the F-layer density profiles in Fig. 9, taken from measurements using the Digisonde installed in SL. It is possible to observe that from 22:00 to 00:00 LT, the F-layer peak height, and peak density decrease. As the F-layer bottom side

476 is at a lower height, it is observed an apparent F-layer uplift, which can be attributed to the
477 recombination process at the bottom side.
478
479 **4.3.3 Es-layer electric fields**
480
481 The role of Es-layer has been considered as a possible cause for the late-time RT instability
482 development. Low-latitude Es-layer can provide enough polarization electric field which
483 maps to equatorial F-layer bottom side, causing F-layer uplift, as pointed out by Yizengaw
484 et al. (2013). They interpreted the occurrence of late plasma irregularities/EPBs over Africa
485 coast during the same period of this work, June solstice 2011, and discussed that during
486 quiet geomagnetic nights, there were favorable conditions for the action of polarization
487 electric fields associated with low-latitude Es-layer/instability which mapped to the
488 equatorial F-layer along the geomagnetic field lines seeding RT-instability and irregularities.
489 In fact, in this work, we can observe the occurrence of the Es-layer at the both quasi-
490 equatorial station FZ and SL, at around 00:00 and 02:50 LT respectively. However, the
491 influence of Es-layers on late time F-layer uplift in this work is not clear since they occur at
492 the same location as the spread-F. Its influence on the post-midnight spread-F during solar
493 minimum is worth of investigation in further works.
494
495 **4.3.4 Mesoscale Travelling Ionospheric Disturbances, MSTIDs and Gravity-Waves,**
496 **GW**
497 MSTIDs have been reported in Brazilian low latitudes using airglow and ionosonde
498 (Candido et al., 2008, 2011; Pimenta et al., 2008). They appear as large-scale dark bands
499 aligned from northeast to southwest propagating northwestward mainly during low solar
500 activity and are associated with electrodynamics forces in mid-latitudes (Perkins instability)

501 or by the propagation of gravity waves in ionospheric heights at low latitudes or equatorial
502 region. If they propagate at equatorial ionospheric heights, they can be seen as oscillations in
503 the F-layer bottom side and can trigger RT-instability and plasma bubbles. In this work, the
504 plasma irregularities seen by the ionosonde are preceded by small oscillations in the F-layer
505 bottom (h'F) and peak heights (hmF2). However, oscillations are usually observed in the F-
506 layer bottom side, and it should be carefully considered in order to establish if they are
507 associated with GWs. Generally, they are considered associated with GW if a downward
508 phase propagation is observed in the fixed frequencies (isolines) plots, i.e., the oscillations
509 are seen firstly in the higher frequencies. Figure 7 showed the occurrence of oscillations in
510 F-layer through some fixed frequencies (isolines) in both stations FZ and SL, although the
511 downward propagation is not precisely apparent. On the other hand, the spread-F pattern
512 observed in this work is quite similar to those reported by Candido et al. (2011) during the
513 descending phase/solar minimum at low latitudes in CP. This feature could suggest that they
514 could be caused by low latitudes MSTIDs propagating equatorward or associated with the
515 action of polarization electric fields mapping from low latitudes MSTIDs structures to the
516 equatorial F-layer bottom side. This kind of event was reported by Miller et al. (2009),
517 which studied the occurrence of EPBs on the same night of the occurrence of MSTIDs
518 propagating in mid-latitudes and attributed them to the action of the electric field from these
519 MSTIDs in the F-layer region. However, the depletions observed in the OI 630-nm emission
520 (Figure 3) present distinct features (propagation direction) of those associated to MSTIDs
521 coming from low latitudes reported by Candido et al. (2011). Also, they are not similar to
522 the depletions associated with the typical EPBs which propagate eastward. Recent results
523 by Takahashi et al. (2018) reported the occurrence of equatorial MSTIDs in high solar
524 activity conditions (2014/15), which were associated with periodic plasma bubbles in the

525 Total Electron Content (TEC) maps in the same region. They showed evidence of
526 tropospheric sources for the development and propagation of GWs at ionospheric heights.
527 Finally, we should address that, as shown in Figs. 2 and 7, late height rise (in both h'F and
528 hmF2) with smaller amplitude waves are observed at SL starting at ~ 21:00 LT when the
529 base height (h'F) increased to > 250 km. Such a condition can be suitable for the growth of
530 RT instability. Over FZ, a similar sequence of variations occurred starting at ~20:00 LT in
531 hmF2. Notice that h'F and hmF2 values were significantly smaller than those at SL.
532 However, it is notable that the oscillations in the F layer heights, especially in hmF2, (with
533 the period around 40 min) that preceded the spread F traces (at both sites) are significantly
534 higher in amplitude at FZ than at SL. This aspect can be noted in more detail in the iso-line
535 plots of plasma frequencies presented in Fig. 7, where the height oscillations show larger
536 amplitudes and occurring at earlier local times at FZ than at SL. Such oscillations may be
537 associated with gravity waves propagating to ionospheric heights with preferential
538 propagating directions to northeast and southeast, as recently reported by Paulino et al.
539 (2016). These oscillations are indicative of the seed perturbations to lead to the spread-F
540 irregularity development through RT mechanism. Depending upon the amplitude of the seed
541 perturbation, even the small increases in the F layer height that marked this period, could be
542 capable of seeding RT instability and consequently generate the spread F irregularities (see,
543 for example, Abdu et al., 2009). To explain the non-local origin of the spread-F traces, as
544 observed at both sites, it will be necessary to assume that the precursor conditions that
545 existed at SL and FZ must have continued to exist in longitude extending further eastward of
546 Fortaleza, perhaps with some increase in intensity so that the irregularities generated therein
547 and drifting westward could be the origin of the oblique spread F trace first observed over
548 FZ and later over SL.
549

It is plausible to consider that the depletions observed in this work can be associated with atypical EPBs triggered by GWs/MSTIDs at locations at the east of FZ and SL or to F-layer uplifts caused by departures from wind system simultaneously to a weakening of the westward zonal electric field (not shown here) during low solar activity. We should notice that the observational techniques used in this work are complementary and validate each other to identify "anomalous" spread-F patterns associated with plasma irregularities/depletions and can help the understanding of the ionosphere during low solar activity. The drift mode is advantageous and suitable for tracking plasma irregularities and their evolution in the absence of other techniques.

5 Summary and Conclusions

In this paper, we have presented and discussed an unusual spread-F pattern associated with unusual depletions on the OI 630.nm airglow emission observed during geomagnetically quiet conditions during the June solstice of 2011 over the equatorial region in Brazil. We summarize our findings as:

1) The unusual spread-F pattern studied in this work presents a distinct feature from those usually observed at post-sunset hours, with spread-F appearing firstly at the higher frequency edge of the F-layer trace to further developing to a mixed (frequency and range) spread-F;

2) The spread-F/depletions occurred during low plasma density conditions, geomagnetically quiet nights, and low solar activity and propagated westward. For the studied case, there is no evidence of previous depletions propagating eastward.

3) The processes to generate spread-F at equatorial latitudes during quiet time seems to be associated with later time F-layer uplifts, possibly caused by departures in the neutral wind system. On its turn, departures in the neutral wind system may be caused by an increased

auroral activity, which in this present study may be associated to the occurrence of a short-duration event of high speed stream (this possible influence is the subject of an ongoing study). Moreover, departures of the wind system associated with a weakening of the westward electric field, or to the propagation of GWs at ionospheric heights, favor the development of the late-time RT-instability. Further studies enclosing simulations are in progress.

4) The spread-F event discussed here presents characteristics similar to those of the earlier cases reported for low latitudes in CP (around the south crest of the EIA), during June solstice of solar minimum 2008-2009 by Candido et al., 2011 and interpreted as the signature of the propagation of mid-latitude MSTIDs in the ionograms.

5) The instrumental approach in this work seems to be suitable for further ionospheric studies, modeling, and forecast during low solar activity.

Abbreviations

SL: Sao Luis

FZ: Fortaleza

CZ: Cajazeira

CP: Cachoeira Paulista

DPS: Digital portable sounder

FPI: Fabry-Perot Interferometer

EPBs: Equatorial plasma bubbles

PMIs: Postmidnight plasma irregularities

RT: Rayleigh-Taylor

EIA: Equatorial ionization anomaly

MSTIDs: Meso-scale traveling ionospheric disturbances

FAIs: Field-aligned irregularities

TIDs: Travelling ionospheric disturbances

SFU: solar flux unity

LT: local time

UT: Universal time

MTM: midnight temperature maximum

GWs: Gravity waves

Data availability

The processed data used in this work can be requested to the author CMNC by the email: claudia.candido@inpe.br. The authors thank to Embrace/INPE Program for the Digisonde raw data which can be downloaded from the website: www.inpe.br/embrace. The airglow and Fabry-Perot data should be requested to the author: JM, by the email: jmakela@illinois.edu.

Author Contributions

CMNC wrote the manuscript and plotted the graphics of the ionospheric parameters. FBG contributed with part of the graphics and revised the manuscript. JS, ISB, EC, MAA, N.B., ZL, CW read and made suggestions to the manuscript. JM and NC provided the airglow figures and Fabry-Perot data and plots, as well as read the manuscript and suggested corrections. All the authors read, commented and made suggestions to the work and agreed with the content and submission of this manuscript.

Competing Interests

The authors declare they have no conflicts of interest.

Acknowledgments

C.M.N.C thanks the Brazilian funding agency CNPq for the financial support through the process n.64537/2015-5, to China-Brazil Joint Laboratory for Space Weather and to China-Brazil Joint Laboratory for Space Weather, CBJLSW, for the postdoctoral fellowship. J. Shi thanks the National Natural Science Foundation of China for the project No. 41674145. Also, the authors thank to Program EMBRACE/INPE/MCTIC for providing ionospheric data to this work. N.P.C. was supported by the NASA Living with a Star Heliophysics Postdoctoral Fellowship Program, administered by the University Corporation for Atmospheric Research (UCAR). Work at the University of Illinois at Urbana-Champaign was supported by National Science Foundation CEDAR grant AGS 09-40253 and was performed in collaboration with J. W. Meriwether at Clemson University. We are grateful to the Universidade Federal de Campina Grande, Pb and to Dr. Ricardo A. Buriti for the support to the imaging systems installed at Cajazeiras.

6 References

Abalde, J. R., Sahai, Y., Fagundes, P. R., Becker-Guedes, F., Bittencourt, J. A. , Pillat, V. G., Lima, W. L. C., Candido, C. M. N., de Freitas, T. F., Day-to-day variability in the development of plasma bubbles associated with geomagnetic disturbances, J. Geophys. Res., 114, A04304, doi:10.1029/2008JA013788, 2009.

Abdu, M. A., Bittencourt, J. A., Batista, I. S., Magnetic declination control of the equatorial F region dynamo field development and spread F, J. Geophys., Res., v. 86, p. 11443-11446, 1981a.

651 Abdu, M. A., Batista, I. S., Bittencourt, J. A., Some characteristics of spread F at the
652 magnetic equatorial station Fortaleza, J. Geophys. Res., 86, A8, 6836-6842, 1981b.
653
654 Abdu, M. A., Sobral, J. H. A., Batista, I. S., Rios, V. H., Medina, C., Equatorial spread F
655 occurrence statistics in the American longitudes: Diurnal, seasonal and solar cycle
656 variations, *Adv. Space Res*., *22*(6), 851–854, 1998.
657
658 Abdu, M. A., Batista, I. S., Reinisch, B. W., de Souza, J. R., Sobral, J. H. A., Pedersen, T.
659 R., Medeiros, A. F., Schuch, N. J., de Paula, E. R., Groves, K. M., Conjugate Point
660 Equatorial Experiment (COPEX) campaign in Brazil: Electrodynamics highlights on spread
661 F development conditions and day-to-day variability, J. Geophys. Res., 114, A04308,
662 doi:10.1029/2008JA013749, 2009.
663
664 Ajith, K. K., Tulasi Ram, S., Yamamoto, M., Otsuka, Y., Niranjan, K., On the fresh
665 development of equatorial plasma bubbles around the midnight hours of June solstice, J.
666 Geophys. Res. Space Physics, 121, 9051–9062, doi:10.1002/ 2016JA023024, 2016.
667
668 Balachandran Nair, R., Balan, N., Bailey, G. J., Rao, P. B., Spectra of the ac electric fields in
669 the post-sunset F-region at the magnetic equator, Planet. Space Sci., 40(5), 655–662.
670 https://doi.org/10.1016/0032-0633(92)90006-A, 1992.
671
672 Balan, N., Jayachandran, B., Balachandran Nair, R., Namboothiri, S. P., Bailey, G. J., Rao,
673 P. B., HF Doppler observations of vector plasma drifts in the evening F-region at the
674 magnetic equator, J. Atmos. Terr. Phys, 54, (11/12), pp. 1545-1554, 1992.
675

676 Balan N., Liu, L. B., Le, H. J., A brief review of equatorial ionization anomaly and
677 ionospheric irregularities, Earth Planet. Phys., 2(4), 1–19.
678 http://doi.org/10.26464/epp2018025, 2018.
679
680 Batista, I. S., de Medeiros, R. T., Abdu, M. A., de Souza, J. R., Equatorial Ionospheric
681 Vertical Plasma Drift Model over the Brazilian Region, J. Geophys. Res., 101 (A5), 10887-
682 10892, 1996.
683
684 Batista, I. S., Abdu, M. A., Carrasco, A. J., Reinisch, B. W., Paula, E. R., Schuch, N. J.,
685 Bertoni, F., Equatorial spread F and sporadic E-layer connections during the Brazilian
686 Conjugate Point Equatorial Experiment (COPEX), J. Atmos. Sol. Terr. Phys., 70, 1133-1143,
687 doi:10.1016/j.jastp.2008.01.007, 2008.
688
689 Booker, H. G., Wells, H. W., Scattering of radio waves in the F-region of the ionosphere,
690 Terr. Magn. Atmos. Electr., 43, 249–256, doi:10.1029/TE043i003p00249, 1938.
691
692 Bowman, G. G., A comparison of nighttime TID characteristics between equatorial
693 ionospheric anomaly crest and midlatitude regions, related to Spread F occurrence, J.
694 Geophys. Res., 106(A2), 1761–1769, doi: 10.1029/2000JA900123, 2001.
695
696 Breit, G., Tuve, M. A., A Test for the Existence of the Conducting Layer, Phys. Rev**.,** 28,
697 pp. 554-575; 1926.
698
699 Calvert, W., Cohen, R., Interpretation and Synthesis of Certain Spread-F Configurations
700 Appearing on Equatorial Ionograms, J. Geophys. Res., 66 (10), 3125-32, 1961.

Candido, C. M. N., Pimenta, A. A., Bittencourt, J. A., Becker-Guedes, F., Statistical analysis of the occurrence of medium-scale traveling ionospheric disturbances over Brazilian low latitudes using OI 630.0 nm emission all-sky images, Geophys. Res. Lett., 35, L17105, doi: 10.1029/2008GL035043, 2008.

Candido, C. M. N., Batista, I. S., Becker-Guedes, F., Abdu, M. A., Sobral, J. H. A., Takahashi, H., Spread F occurrence over a southern anomaly crest location in Brazil during June solstice of solar minimum activity, J. Geophys. Res., 116, A06316, Doi:10.1029/2010JA016374, 2011.

Chapagain, N. P., Makela, J. J., Meriwether, J. W., Fisher, D. J., Buriti, R. A., Medeiros, A. F., Comparison of Nighttime Zonal Neutral Winds and Equatorial Plasma Bubble Drift Velocities over Brazil, J. Geophys. Res., doi: 10.1029/2012JA017620, 2012.

Dao, T., Otsuka, Y., Shiokawa, K., Tulasi Ram, S., Yamamoto, M., Altitude development of postmidnight F region field-aligned irregularities observed using Equatorial Atmosphere Radar in Indonesia, Geophys. Res. Lett., 43, 1015–1022, doi:10.1002/ 2015GL067432, 2016.

Fisher, D. J., Makela, J. J., Meriwether, J. W., Buriti, R. A., Benkhaldoun, Z., Kaab, M., Lagheryeb, A., Climatologies of nighttime thermosphericwinds and temperatures fromFabry-Perot interferometer mea-surements: From solar minimumto solar maximum, J. Geophys. Res.Space Physics, 120, 6679–6693,doi:10.1002/2015JA021170, 2015.

726 Galkin, I. A., Khmyrov, G. M., Reinisch, B. W., McElroy, J., The SAOXML 5: New format
727 for ionogram-derived data, in Radio Sounding and Plasma Physics, AIP Conf. Proc. 974,
728 160-166, 2008.
729
730 Heisler, L. H., Anomalies in ionosonde records due to traveling ionospheric disturbances,
731 Austr. J. Phys., V.11, pp. 79, 1958.
732
733 Li, G., Ning, B., Abdu, M. A., Yue, X, Liu, L. Wan, W., Hu, L., On the occurrence of
734 postmidnight equatorial F region irregularities during the June solstice, J. Geophys. Res.,
735 116, A04318, doi:10.1029/2010JA016056, 2011.
736
737 MacDougall, J. W., Abdu, M.A., Jayachandran, P. T., Cecile, F., Batista, I. S., Presunrise
738 spread F at Fortaleza, J. Geophys. Res., 103 (A10), 23415-23425, 1998.
739
740 MacDougall, J., Abdu, M. A., Batista, I., Buriti, R., Medeiros, A. F., Jayachandran, P. T.,
741 and Borba, G., Spaced transmitter measurements of medium-scale traveling ionospheric
742 disturbances near the equator, Geophys. Res. Lett., 38, L16806,
743 Doi:10.1029/2011GL048598, 2011.
744
745 Makela, J. J., Miller, E. S., Optical observations of the growth and day-to-day variability of
746 equatorial plasma bubbles, J. Geophys. Res., 113, A03307, doi:10.1029/2007JA012661,
747 2008.
748

749 Makela, J. J., Miller, E. S., Tallat, E., Nighttime medium-scale traveling ionospheric
750 disturbances at low geomagnetic latitudes, Geophys. Res. Lett., 37, L24104,
751 doi:10.1029/2010GL045922, 2010.
752
753 Miller, E. S., Makela, J. J., Kelley, M. C., Seeding of equatorial plasma depletions by
754 polarization electric fields from middle latitudes: Experimental evidence, Geophys. Res.
755 Lett., 36, L18105, doi:10.1029/2009GL039695, 2009.
756
757 Munro, G. H., Heisler, L. H., Cusp-Type Anomalies in Variable Frequency Ionospheric
758 Records, Austr. J. of Physics, V.9 (3), 343-358, 1956.
759
760 Nicolls, M. J, Kelley, M. C., Vlasov, M. N., Sahai, Y., Chau, J. L., Hysell, D. L., Fagundes,
761 P. R., Becker-Guedes, F., Lima, W. L. C., Observations and modeling of post-midnight
762 uplifts near the magnetic equator, Ann. Geophysicae, 24, 1,317–1,331, 2006.
763
764 Nishioka, M., Otsuka, Y., Shiokawa, K., Tsugawa, T., Effendy, Supnithi, P., Nagatsuma, T.,
765 Murata, K. T., On post-midnight field-aligned irregularities observed with a 30.8-MHz radar at a
766 low latitude: Comparison with F-layer altitude near the geomagnetic equator, J. Geophys. Res.,
767 117, A08337, 732 doi:10.1029/2012JA017692, 2012.
768
769 Otsuka, Y., Ogawa, T., Effendy, VHF radar observations of nighttime F-region field-aligned
770 irregularities over Kototabang, Indonesia, Earth Planets Space, 61(4), 431-437, 2009.
771
772 Otsuka, Y., Review of the generation mechanisms of post-midnight irregularities in the
773 equatorial and low-latitude ionosphere, Progress in Earth and Planetary Science, 5:57
774 https://doi.org/10.1186/s40645-018-0212-7, 2017.

Paulino, I., Medeiros, A. F., Buriti, R. A., Sobral, J. H. A., Takahashi, H., Gobbi, D, Optical observations of plasma bubble westward drift over Brazilian tropical region, J. Atmos. Terr. Phys, V. 72 (5-6), 521-27, 2010.

Paulino, I., Medeiros, A. F., Vadas, S., Wrasse, C. M., Takahashi, H., Buriti, R. A., Leite, D., Figueira, S., Bageston, J. V., Sobral, J.H.A., Gobbi, D., Periodic waves in the lower thermosphere observed by OI630nm airglow images. Ann. Geophys., 34, 293–301, 2016.

Pimenta, A. A., Amorim, D., Candido, C. M. N., Thermospheric dark band structures at low latitudes in the Southern Hemisphere under different solar activity conditions: A study using OI 630 nm emission all-sky images, Geophys. Res. Lett., 35, p. L16103, doi:10.1029/2008GL034904, 2008.

Ratcliffe, J. A., Some Irregularities in the F2 Region of the Ionosphere, J. Geophys. Res., 50(4), 487-507, 1956.

Reinisch, B. W., Abdu, M. A., Batista, I. S., Sales, G. S., Khmyrov, G., Bullett, T. A., Chau, T., Rios, V., Multistation digisonde observations of equatorial spread F in South America, Ann. Geophys., 22, 3145–3153, 2004.

Reinisch, B. W., Huang, X., Galkin, I. A., Paznukhov, V., Kozlov, A., Recent advances in the real-time analysis of ionograms and ionospheric drift measurements with digisondes, J. Atmos. Terr. Phys., 67 (2005) 1054–1062, 2005.

Sahai, Y., Fagundes, P. R., Bittencourt, J. A, Transequatorial F-region ionospheric plasma bubbles solar cycle effects, Journal of Atmospheric and Solar-Terrestrial Physics, 62: 1377-1383, 2000.

Sobral, J. H. A., Abdu, M. A,; Takahashi, H., Taylor, M. J., de Paula, E. R., Zamlutti, C. J., Aquino, M. G.; Borba, G. L., Ionospheric plasma bubble climatology over Brazil based on 22 years (1977-1998) of 630 nm airglow observations, Journal of Atmospheric and Solar-Terrestrial Physics, 64: 1517-1524, 2002.

Sobral, J. H. A., deCastilho, V. M., Abdu, M. A., Takahashi, H., Paulino, I, Gasparelo, U. A. C., Arruda, D. C. S., Mascarenhas, M., Zamlutti, C. J., Denardini, C. M., Koga, D., deMedeiros, A. F., Buriti, R. A., Midnight reversal of ionospheric plasma bubble eastward velocity to westward velocity during geomagnetically quiet time: Climatology and its model validation, J. Atmos. Terr. Phys., 73, 1520–1528, 2011.

Takahashi, H., Wrasse, C. M., Figueiredo, C. A. O. B., Barros, D., Abdu, M.A., Otsuka, Y., Shiokawa, K., Equatorial plasma bubble seeding by MSTIDs in the ionosphere, Progress in Earth and Planetary Science, 5:32, 2018.

Valladares, C. E., Hanson, W. B., McClure, J. P., Cragin, B .L., Bottomside sinusoidal irregularities in the equatorial F region, Journal of Atm. and Solar-Terr Phys, V. 88 (A10), https://doi.org/10.1029/JA088iA10p08025, 1983.

Yizengaw, E., Retterer, J., Pacheco, E. E., Roddy, P., Groves, K., Caton, R., Baki, P., Postmidnight bubbles and scintillations in the quiet-time June solstice, Geophys. Res. Lett., 40, doi:10.1002/2013GL058307, 2013.

Yokoyama, T., Yamamoto, M., Otsuka, Y., Nishioka, M., Tsugawa, T., Watanabe, S. and Pfaff, R. F., On post-midnight low latitude ionospheric irregularities during solar minimum: 1. Equatorial Atmosphere Radar and GPS TEC observations in Indonesia, J. Geophys. Res., 116, A11325, doi:10.1029/2011JA016797, 2011.

Zhan, W., Rodrigues, F., Milla, M., On the genesis of postmidnight equatorial spread *F*: Results for the American/Peruvian sector, Geophysical Research Letters, 45, 7354–7361. https://doi.org/10.1029/2018GL078822, 2018.

848

849

850

851

852

853

854

855

856

857

858

859

860

861

862

863

864

865

866

867

868

869

870

871

872

873 Figure 1

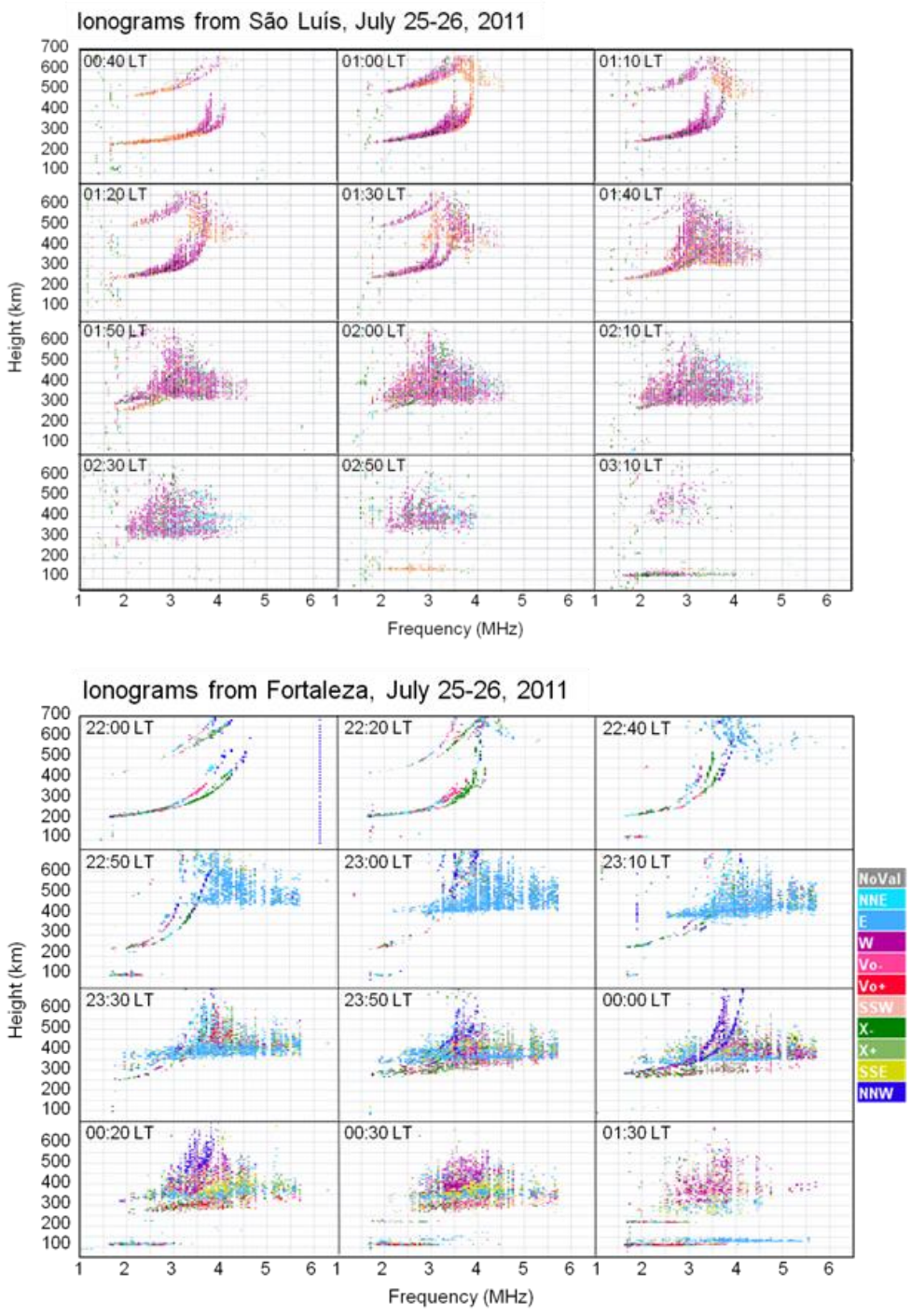

874

875

876 **Figure 1**: Sequence of ionograms obtained on July 25-26, at Sao Luis, SL, from 00:40 to
877 03:10 LT and over Fortaleza, FZ, Brazil, 2011, from 22:00 to 01:30 LT. The spread-F shows
878 an unusual pattern, with oblique echoes. The color scale in FZ ionograms indicates echoes
879 are coming from the east and propagating westward.

880 Figure 2

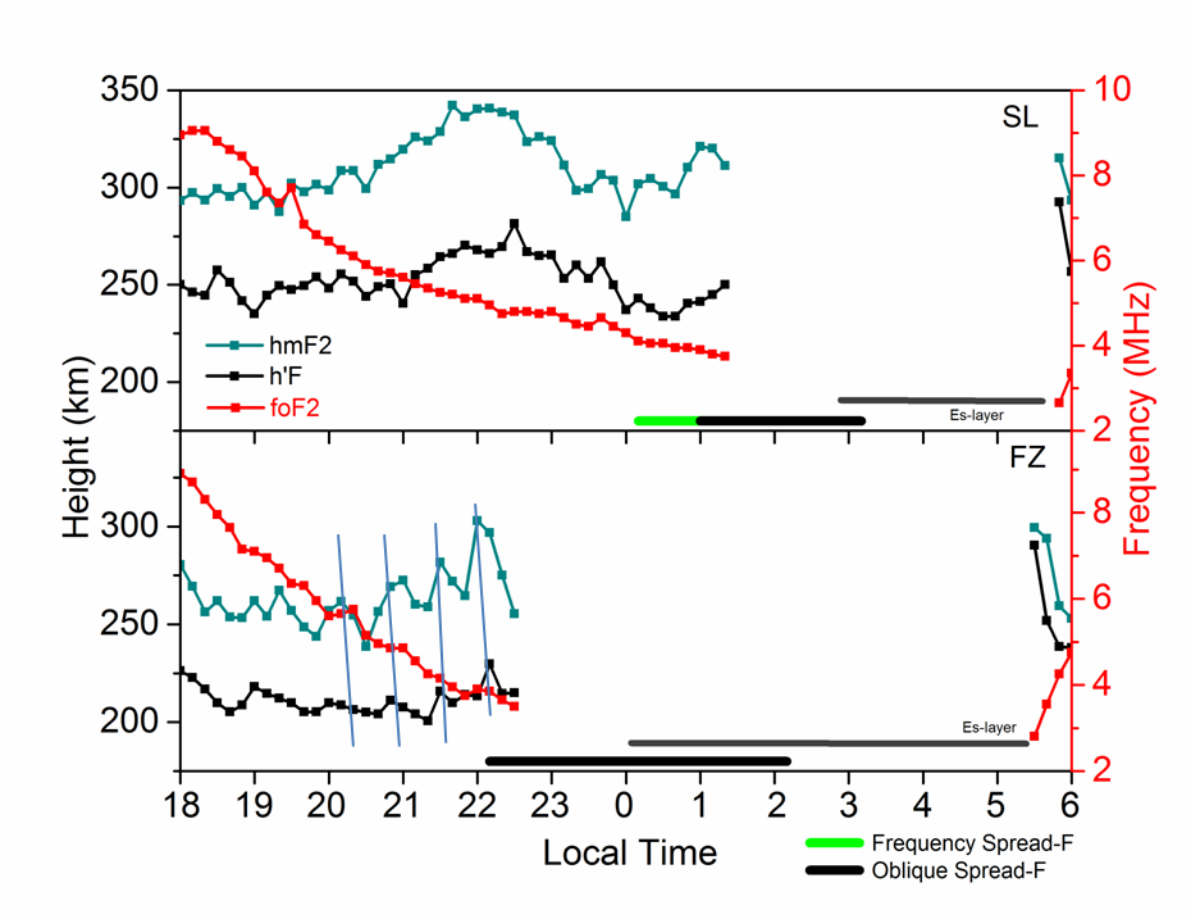

881

882 **Figure 2**: F-layer parameters h'F (km), hmF2 (km) and foF2 (MHz), on July 25-26, 2011

883 obtained from the Digisondes at SL (top panel) and FZ (bottom panel).

884

885

886

887

888

889

890

891

892

893 Figure 3

894

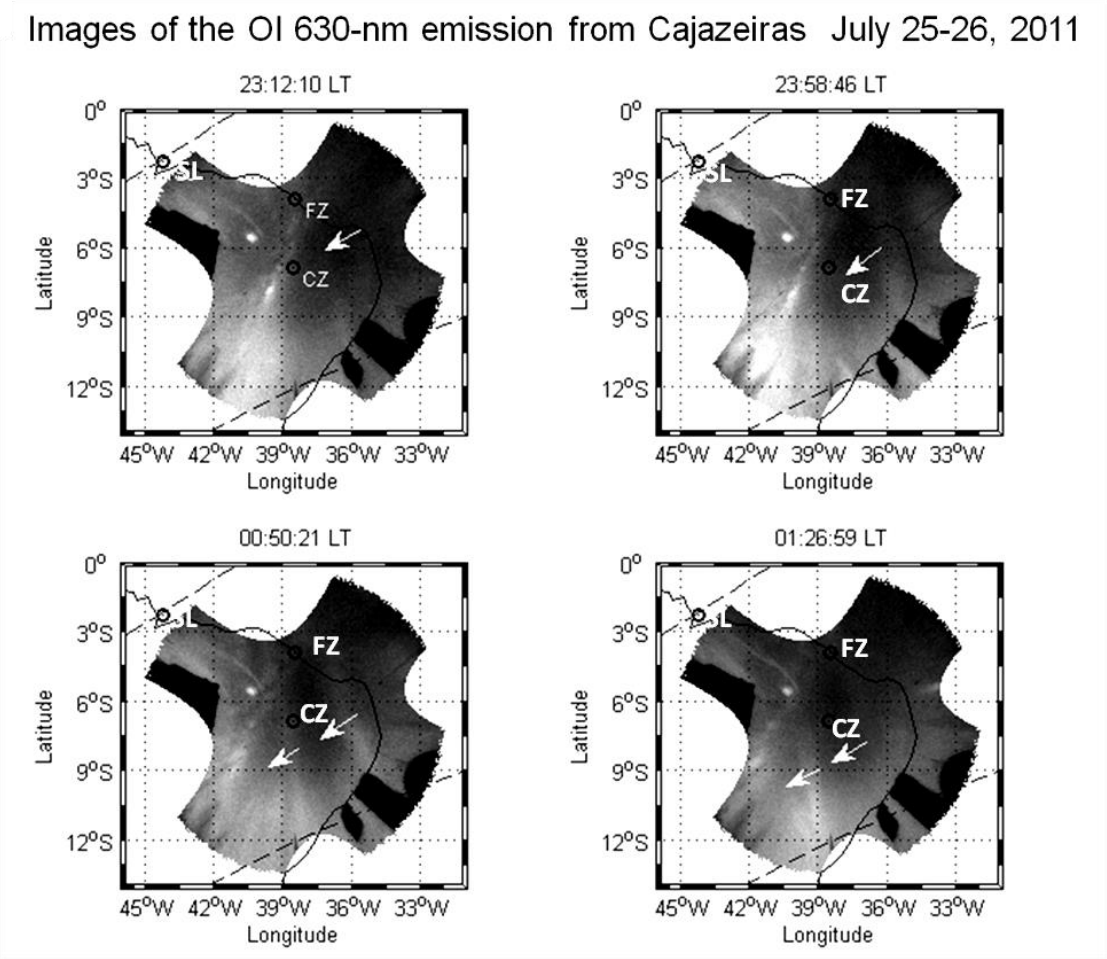

895

896 **Figure 3**: Sequence of OI 630-nm images showing the time evolution of depletions on July
897 25-26, 2011, between 23:12 LT and 01:26 LT at Cajazeiras, Brazil. The images are
898 projected onto geographic coordinates over the Brazil map. In the plot, FZ is Fortaleza, SL
899 is Sao Luis, and CZ is Cajazeiras. Arrows indicate the propagation direction of the
900 depletions (dark regions passing over FZ and CZ).

901

902

903

904

905

Figure 4

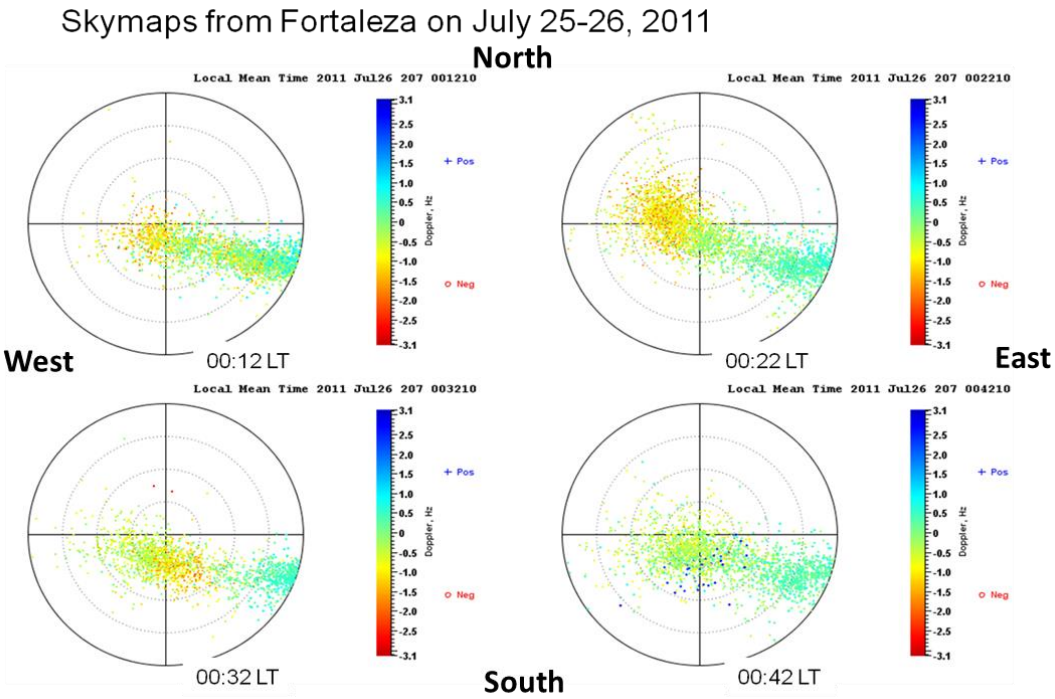

Figure 4: Skymaps registered over FZ from 00:12 LT to 00:42 LT on July 26, 2011, showing the echoes location and Doppler frequencies (color-coded) for F-region echoes from Digisondes. Doppler velocities are positive (negative) for irregularities arriving (leaving) the station.

922 Figure 5

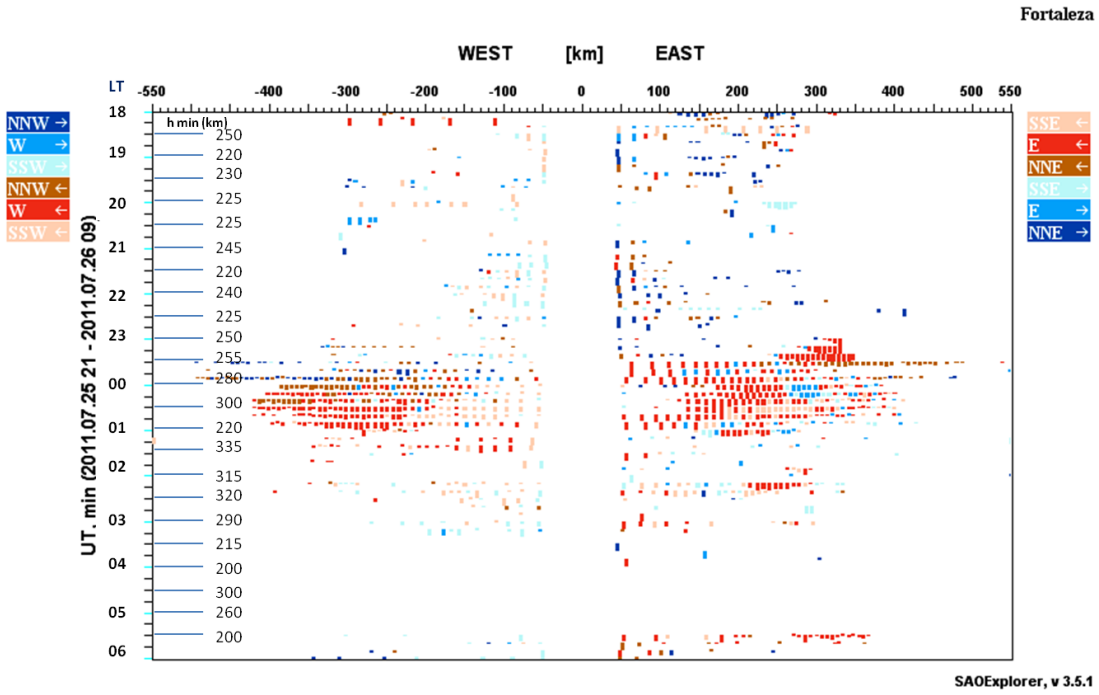

923

924

925 **Figure 5:** Directogram for Fortaleza on July 26 showing the location and the horizontal
926 distances of the irregularities detected by Digisonde and seen in the ionograms as spread-F.
927 At left is shown the F-region height (km), where hmin is the spread-F reflection height.
928 Color code with arrows indicates the direction where the irregularities are coming from or
929 where the irregularities are moving to.

930

931

932

933

934

935

936

937

938 Figure 6

939

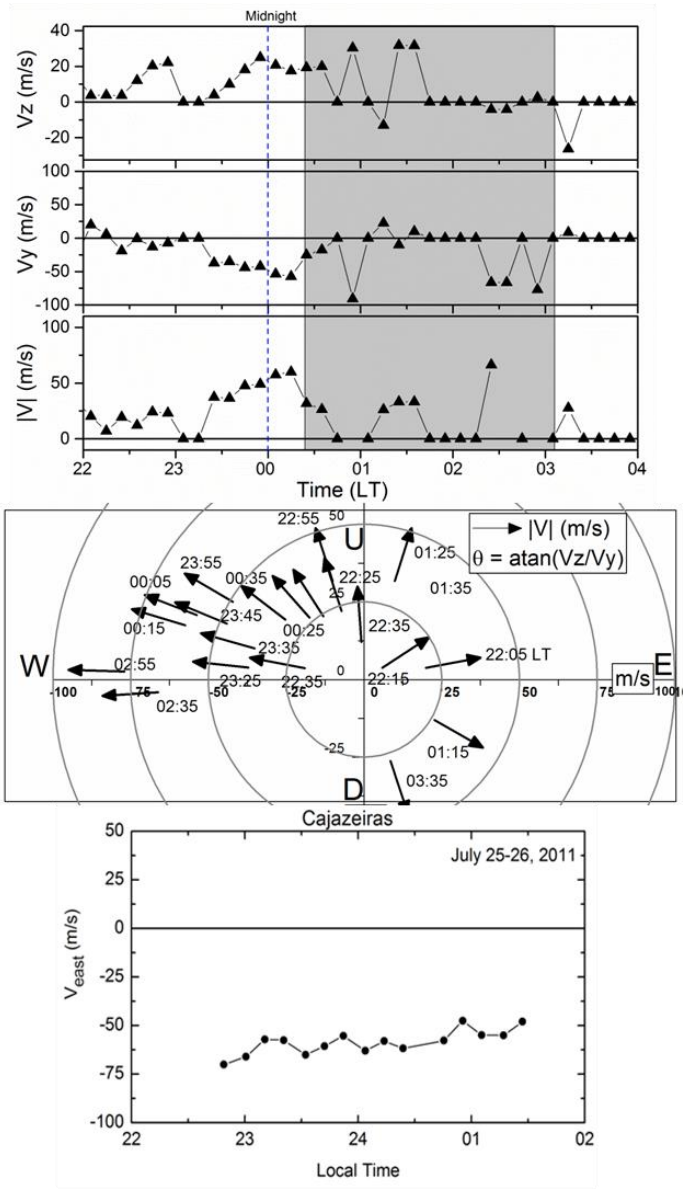

940

941 Figure 6: Top panel: vertical (Vz), zonal (Vy), and total (|V|) drift velocities on July 25-26,
942 2011 over FZ from 22:00 LT to 04:00 LT. $V_y > 0$ is eastward. Middle panel: vector diagram
943 showing the variations and directions of the mean total drift velocity of the irregularities
944 seen as spread-F in ionograms. For clarity, the |V| values are represented by the arrow start
945 points. Bottom panel: Zonal drift velocities obtained from the depletions seen on the OI
946 630.0 nm emission images obtained at CZ on July 25-26, 2011 for comparison.

947

948 Figure 7

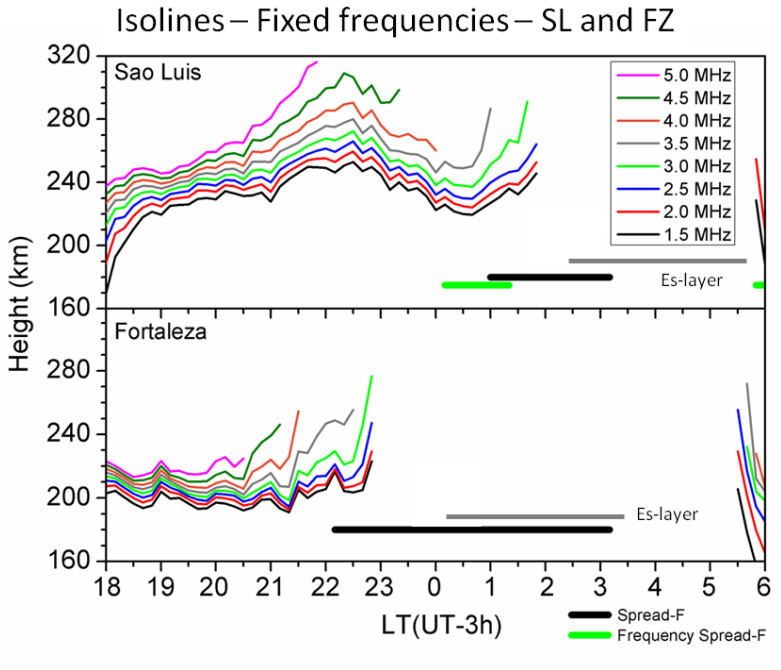

949

950 Figure 7: Oscillations in the real height of F-layer at fixed frequencies (1.5 to 5.0 MHz)

951 before the spread-F in Sao Luis (top panel) and Fortaleza (bottom panel).

952

953

954

955

956

957

958

959

960

961

962

963

964

965 Figure 8

966

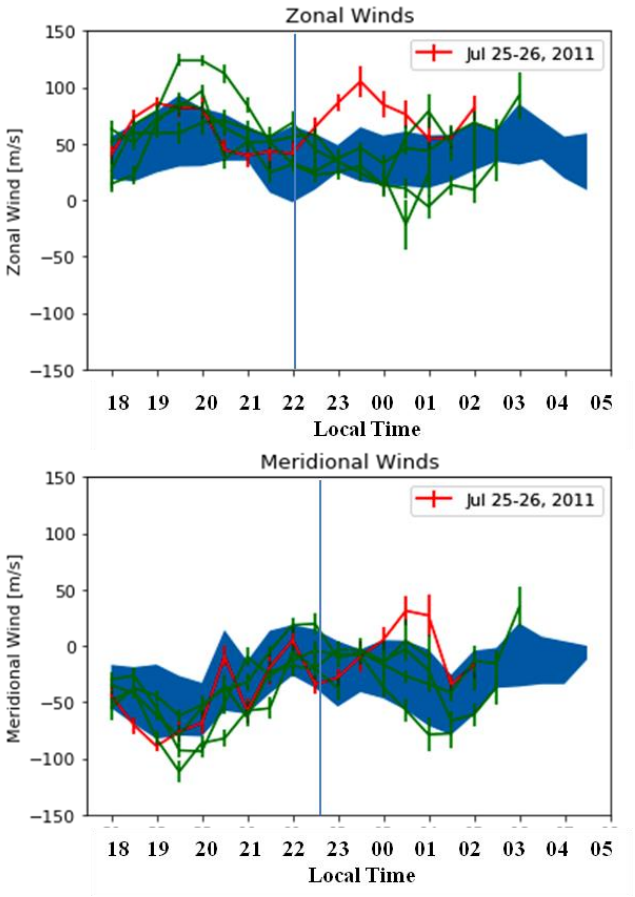

967

968 Figure 8: Measured Zonal and Meridional Winds in CZ, Brazil, in 25-26 July 2011. The
969 shaded region is the monthly average with standard deviation, the green lines are the mean
970 winds on July 25-26 (mean of 2 days), and the red line is for July 25-26.

971

972

973

974

975

976

977

978

Figure 9

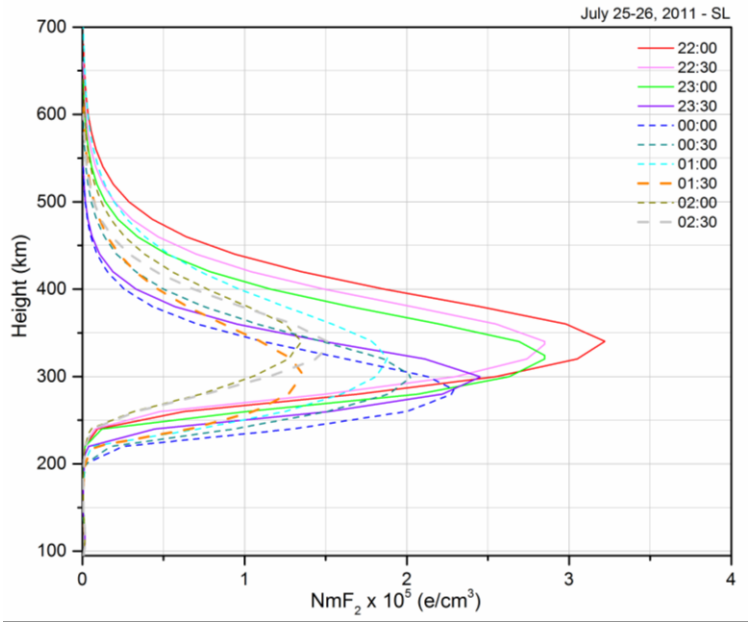

Figure 9: F-layer plasma density profile for July 25-26 derived from Digisonde data and SAO Explorer data for several hours (LT).

996 **List of Figures**

997

998 **Figure 1**: Sequence of ionograms obtained on July 25-26, at Sao Luis, SL, from 00:40 to
999 03:10 LT and over Fortaleza, FZ, Brazil, 2011, from 22:00 to 01:30 LT. The spread-F shows
1000 an unusual pattern, with oblique echoes. The color scale in FZ ionograms indicates echoes
1001 are coming from the east and propagating westward.

1002

1003 **Figure 2**: F-layer parameters h'F (km), hmF2 (km) and foF2 (MHz), on July 25-26, 2011
1004 obtained from the Digisondes at SL (top panel) and FZ (bottom panel).

1005

1006 **Figure 3**: Sequence of OI 630-nm images showing the time evolution of depletions on July
1007 25-26, 2011, between 23:12 LT and 01:26 LT at Cajazeiras, Brazil. The images are
1008 projected onto geographic coordinates over the Brazil map. In the plot, FZ is Fortaleza, SL
1009 is Sao Luis, and CZ is Cajazeiras. Arrows indicate the propagation direction of the
1010 depletions (dark regions passing over FZ and CZ).

1011

1012 **Figure 4**: Skymaps registered over FZ from 00:12 LT to 00:42 LT on July 26, 2011,
1013 showing the echoes location and Doppler frequencies (color-coded) for F-region echoes
1014 from Digisondes. Doppler velocities are positive (negative) for irregularities arriving
1015 (leaving) the station.

1016

1017 **Figure 5:** Directogram for Fortaleza on July 26 showing the location and the horizontal
1018 distances of the irregularities detected by Digisonde and seen in the ionograms as spread-F.
1019 At left is shown the F-region height (km), where hmin is the spread-F reflection height.

Color code with arrows indicates the direction where the irregularities are coming from or where the irregularities are moving to.

Figure 6: Top panel: vertical (Vz), zonal (Vy), and total (|V|) drift velocities on July 25-26, 2011 over FZ from 22:00 LT to 04:00 LT. $V_y > 0$ is eastward. Middle panel: vector diagram showing the variations and directions of the mean total drift velocity of the irregularities seen as spread-F in ionograms. For clarity, the |V| values are represented by the arrow start points. Bottom panel: Zonal drift velocities obtained from the depletions seen on the OI 630.0 nm emission images obtained at CZ on July 25-26, 2011 for comparison.

Figure 7: Oscillations in the real height of F-layer at fixed frequencies (1.5 to 5.0 MHz) before the spread-F in Sao Luis (top panel) and Fortaleza (bottom panel).

Figure 8: Measured Zonal and Meridional Winds in CZ, Brazil, in 25-26 July 2011. The shaded region is the monthly average with standard deviation, the green lines are the mean winds on July 25-26 (mean of 2 days), and the red line is for July 25-26.

Figure 9: F-layer plasma density profile for July 25-26 derived from Digisonde data and SAO Explorer data for several hours (LT).